Plant Science 273 (2018) 50–60

Contents lists available at ScienceDirect

Plant Science

journal homepage: www.elsevier.com/locate/plantsci

From reconstruction to C_4 metabolic engineering: A case study for overproduction of polyhydroxybutyrate in bioenergy grasses☆

Cristiana Gomes de Oliveira Dal'Molin[a,*,1], Lake-Ee Quek[b,1], Pedro A. Saa[c,d], Robin Palfreyman[a], Lars Keld Nielsen[a,e]

[a] Australian Institute for Bioengineering and Nanotechnology, School of Chemical Engineering, University of Queensland, Brisbane, Queensland 4072, Australia
[b] School of Mathematics and Statistics, The University of Sydney, New South Wales 2006, Australia
[c] Department of Chemical and Bioprocess Engineering, Pontificia Universidad Católica de Chile, Santiago, Casilla 306, Correo 22, Chile
[d] Mathomics, Center for Mathematical Modeling, Universidad de Chile, Santiago, Chile
[e] Novo Nordisk Foundation Center for Biosustainability, The Technical University of Denmark, Lyngby, DK-2800, Denmark

ARTICLE INFO

Keywords:
PHB sink
Diurnal cycle
C_4 modelling
Metabolic reconstruction

ABSTRACT

The compartmentalization of C_4 plants increases photosynthetic efficiency, while constraining how material and energy must flow in leaf tissues. To capture this metabolic phenomenon, a generic plant metabolic reconstruction was replicated into four connected spatiotemporal compartments, namely bundle sheath (B) and mesophyll (M) across the day and night cycle. The C_4 leaf model was used to explore how amenable polyhydroxybutyrate (PHB) production is with these four compartments working cooperatively. A strategic pattern of metabolite conversion and exchange emerged from a systems-level network that has very few constraints imposed; mainly the sequential two-step carbon capture in mesophyll, then bundle sheath and photosynthesis during the day only. The building of starch reserves during the day and their mobilization during the night connects day and night metabolism. Flux simulations revealed that PHB production did not require rerouting of metabolic pathways beyond what is already utilised for growth. PHB yield was sensitive to photoassimilation capacity, availability of carbon reserves, ATP maintenance, relative photosynthetic activity of B and M, and type of metabolites exchanged in the plasmodesmata, but not sensitive towards compartmentalization. Hence, the compartmentalization issues currently encountered are likely to be kinetic or thermodynamic limitations rather than stoichiometric.

1. Introduction

C_4 plants are resilient to harsh growth conditions. Although CO_2 assimilation costs more energy (ATP), C_4 plants can have five times higher yield than C_3 plants under drought, high temperature or limiting CO_2 conditions [1,2]. C_4 photosynthesis is an evolutionary development where photosynthesis becomes a cooperative process between two types of cells, the mesophyll (M) and the bundle sheath (B), to avoid photorespiration (Fig. 1) [3]. CO_2 is shuttled from M to B *via* a 4-carbon dicarboxylic acid, thus concentrating CO_2 where the RuBisCO enzyme resides. The use of bioenergy C_4 grasses, like sugarcane and switchgrass, as biofactories to produce 'green', high-value chemicals or biopolymers is attractive because these industrial crops can be cultivated at scale using modern agricultural technologies [4–9].

We have genetically engineered sugarcane [7,10–12] and switchgrass [5,13,14] for the production of the biodegradable polymer polyhydroxybutyrate (PHB) in leaves. The PHB pathway consists of three enzymatic reactions and utilises acetyl-CoA as metabolic substrate. In the first step reaction, ß-ketothiolase (PhbA; EC 2.3.1.16) condenses two molecules of acetyl-CoA to acetoacetyl-CoA. In the second step, acetoacetyl-CoA reductase (PhbB; EC 1.1.1.36) catalyses the formation of 3-hydroxybutyryl-CoA with the cost of NADPH. The final step is the polymerisation of 3-hydroxybutyryl-CoA monomers into PHB by P(3HB) polymerase (PhbC). While it is possible to make PHB in various leaf organelles [7,15], chloroplast targeting has yielded the best production lines [6,11].

We can reliably overexpress the PHB pathway in chloroplasts [6,11] (Fig. 1, step 10 and 11), but C_4 engineering is inevitably tied to adverse phenotypes such as stunted growth and reduced biomass yield, particularly with yields above ~1.5% dry weight [6,10–12]. The abnormal growth of PHB producer lines drew our attention to unknown metabolic penalties

☆ This article is part of a special issue entitled "Synthetic biology meets plant metabolism", published in the journal Plant Science 273, 2018.

* Corresponding author.
E-mail address: c.gomesdeoliveira@uq.edu.au (C. Gomes de Oliveira Dal'Molin).

[1] These authors contributed equally to this work.

https://doi.org/10.1016/j.plantsci.2018.03.027
Received 19 December 2017; Received in revised form 27 February 2018; Accepted 1 March 2018
Available online 05 April 2018

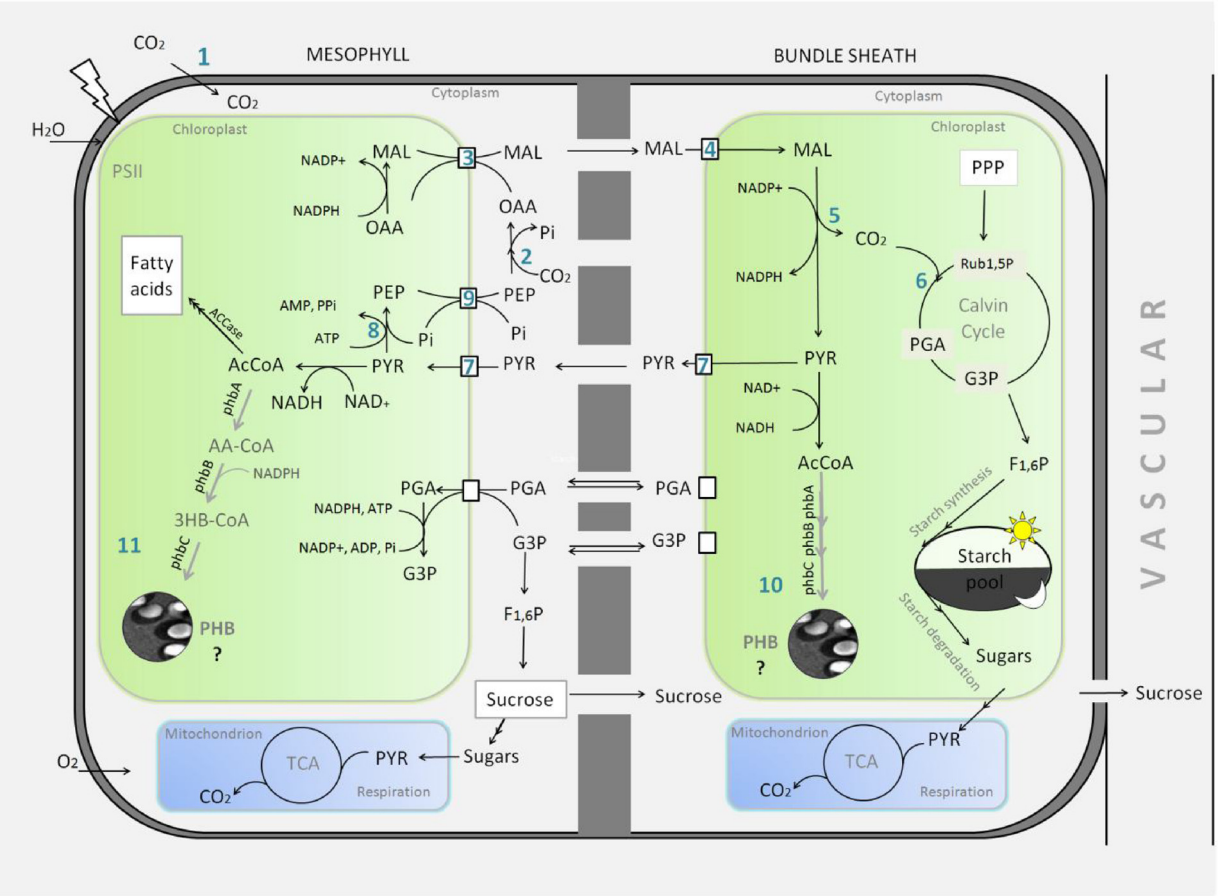

Fig. 1. C_4 photosynthesis and targeted pathways for PHB synthesis in mesophyll and bundle sheath chloroplasts. The following steps represent C_4 photosynthesis of a NADP-ME subtype. Steps 1–9 represent the cooperative C_4 photosynthesis in mesophyll and bundle sheath cells. Steps 10 and 11 show PHB synthesis in bundle sheath and mesophyll chloroplast, respectively. Steps 1–2: carbon assimilation; steps 3–4: C_4 acids translocation *via* plasmodesmata; step 5: decarboxylation *via* NADP-malic enzyme and CO_2 concentration in bundle sheath; step 6: CO_2 fixation in Calvin cycle; step 7: 3C compound translocation from bundle sheath to mesophyll *via* plasmodesmata.

Table 1
Starch and sucrose content in leaves of wild type and PHB-producing sugarcane and switchgrass plants.

Species	Species	Starch (%)	Sucrose (%)	Total C reserve (%)
Switchgrass	WT	1.19 ± 0.34	3.16 ± 0.50	**4.35**
	HP	0.2 ± 0.07	1.58 ± 0.39	**1.78**
Sugarcane	WT	2.15 ± 0.54	4.68 ± 0.53	**7.18**
	HP	0.14 ± 0.06	0.97 ± 0.14	**1.11**

Values are presented in percentage of leaf dry weight ± standard deviation. WT, wild type; HP, high producer (PHB > 2%DW). Original results are reported by McQualter et al. [11].

incurred by PHB producer lines, such as depleted intracellular starch and sucrose (Table 1) and reduced photoassimilation capacity [6,10,13] [11]. We speculate that high producer lines were unhealthy because they lacked carbon reserves to sustain metabolism across the diurnal cycle.

Surprisingly, PHB is produced solely in B chloroplasts even in the best production lines [6,11]. Leaf real estate is thus underutilised because the leaf is predominantly M cells. It is neither poor targeting nor inactivity of the PHB enzymes that limits PHB production in M chloroplasts [6,11], nor precursor limitations because fatty acid content was unaffected [11]. The production in M can be coaxed by promoting the conversion of the acetyl-CoA into PHB using an ACCase inhibitor or by replacing ß-ketothiolase with acetoacetyl-CoA synthase (EC 2.3.1.19, *NphT7)* [16,12]. The metabolic network stoichiometry and connectivity may explain the bias of PHB production between B and M cells given that the cells have different metabolic capabilities.

Our struggles to reach economically viable yields (minimum of 10% PHB on a leaf dry weight basis) [6,10,13] are constant reminders that engineering a novel carbon sink in plants is not simply achieved by overexpressing the pathway. A systems approach is required to guide future metabolic engineering strategies [17,18,19]. Here, we applied genome-scale metabolic network analysis to determine the underlying causes of growth retardation and the apparent PHB production inefficiency in M plastids [17,20]. MultiGEM (a multi-tissue metabolic modelling framework) was used to understand metabolic consequences of PHB production in the context of two metabolically different cell types in leaf operating on a day-night cycle [21]. We tested (i) the limitations of carbon reserves and photoassimilation efficiency, (ii) metabolic demands of diurnal cycles, and (iii) pathways that are strongly coupled to PHB production. C_4 plants show remarkable metabolic flexibility, but are physiologically constrained to the specialization/division-of-labour of B and M cells, and the availability of light, CO_2, and carbon reserves. To our knowledge, this is the first study to combine the use of plant metabolic reconstruction and spatiotemporal modelling to investigate overproduction of PHB in C_4 leaves.

2. Material and methods

2.1. C_4 leaf diurnal metabolism

In C_4 carbon fixation (Fig. 1), phosphoenolpyruvate carboxylase (PEPC) in specialised M cells fixes CO_2 into 4-carbon dicarboxylic acids

(*e.g.*, oxaloacetate, malate or aspartate), which are then transported *via* plasmodesmata to B cells (Fig. 1, steps 2–4). CO_2 is released from the dicarboxylic acids in B and concentrated [22]; the conjugated 3-carbon acids are transported back into M (Fig. 1, step 5, 7). CO_2 is then assimilated by the Calvin cycle in B chloroplasts (Fig. 1, step 6) to produce 3-phosphoglycerate, which can be reduced to glyceraldehyde 3-phosphate (G3P). Central metabolism converts the latter to ribose, hexose, starch, sucrose, and other carbohydrates, which feed other non-photosynthetic tissues *via* the plant's vascular system [23].

During the day, leaf metabolism is driven by the availability of light and free CO_2, subsequently shifting to oxidative respiration in the absence of light. Light-dependent reactions produce the required NADPH and ATP, with additional ATP provided by cyclic photophosphorylation. Plant growth and maintenance at night, however, are sustained by catabolism of carbon reserves; ATP and NAD(P)H are produced by glycolysis and *via* the TCA cycle. Here, starch granules are treated as the main carbon reserve, and are synthesised and stored in B cells (Fig. 1) [24].

Leaf specific growth rate was assumed to be 0.11 day^{-1} [25]. The metabolic burden of PHB production is thus evaluated relative to growth demands.

2.2. MultiGEM for spatiotemporal genome-scale modelling

In silico simulations are essential when exploring complex, multi-organelle and multi-tissue metabolic systems [17,20]. Plant genome-scale metabolic reconstructions are well established [9,26–31], and have advanced from single cell to multi-tissue/whole plant modelling [21,27,32]. Potential applications include the investigation of carbon partitioning and solving metabolic engineering problems [33]. The modelling framework is relatively fast to implement and scalable. A metabolic reconstruction captures the full potential of a cell, and interrogation models are generated from the reconstruction to test hypotheses and to identify useful engineering strategies [17–19,33], *e.g.*, pathway alteration to improve product yield. More importantly, the model context must be correctly framed; in our case, making PHB in the C_4 leaf over a 24 h period.

MultiGEM is a framework to propagate a single reconstruction into many spatiotemporal compartments, with users separately specifying the connections between compartments and the metabolic constraints for each compartment [21]. Here, MultiGEM was used to simulate C_4 and diurnal metabolism from a primary plant metabolic reconstruction, AraGEM [26]. This is an improvement over C4GEM [27], which has metabolic connections and compartmentalization hard-coded into the SBML reconstruction, and is not easily modified. MultiGEM provides the flexibility to add multiple tissue compartments (*e.g.*, B-day, B-night, M-day and M-night), to specify allowable boundary exchanges for each compartment (*e.g.*, sucrose exported to vascular *via* B), to specific flux capacity of a reaction in a specific compartment (*e.g.*, no RuBisCO in B), and to connect metabolites between compartments in a spatiotemporal fashion (*e.g.*, malate, starch).

Fig. 2A illustrates the MultiGEM workflow. Briefly, MultiGEM reads a plant reconstruction of choice (in sbml format) (step 1). Flux constraints (*e.g.*, on/off reaction or transporter) are introduced to the network to represent tissue-specific metabolic capabilities (step 2) [27], and can be derived from transcriptome, proteome or biochemical studies. The tissue models are then connected by introducing spatial and temporal transport compartments, defined as common pool (CP) and storage pool (SP), respectively, which describe the balanced exchanges between two or more compartments (step 3). Conceptually the same, CP models the spatial exchanges *via* plasmodesmata, and SP models the starch accumulation and subsequent mobilization over the day-night cycle. Both CP and SP are balanced, *i.e.*, no net accumulation. The CP metabolites are malate, pyruvate, phosphoenolpyruvate, alanine, aspartate, sucrose phosphate, glycerone phosphate, glyceraldehyde-3-phosphate, CO_2, and O_2. In MATLAB, MultiGEM reads information tabulated plainly in a "model specification" spreadsheet, and generates the required stoichiometric matrix and lower/upper boundary values (see Supplementary file, MultiGEM package).

2.3. Flux balance analysis and hypothesis testing

The C_4 leaf model was generated by replicating AraGEM into multiple stoichiometric models, and strategically connecting each model's internal metabolites to boundary and shared (spatially or temporally) metabolites (Eq. (2)). The stoichiometric matrix S represents AraGEM [26], which includes inter-organelle transporters, but is replicated into four instances S_{MD}, S_{MN}, S_{BD}, and S_{BN} to represent the four tissue-diurnal compartments: M-day, M-night, B-day, and B-night. Allowable boundary exchanges E were created for each compartment to represent the transport of metabolites with environment. These exchange reactions were weighted based on the spatiotemporal mass fraction $\omega_{\text{spatiotemporal}}$ of the compartments (Eq. (2)). Similarly, spatially and temporally shared metabolite pools were assigned, but these pools were balanced by CP = 1 and SP = 1. $\omega_{\text{spatiotemporal}}$ was again used to connect CP and SP with the respective intracellular metabolites. $\omega_{\text{spatiotemporal}}$ is the product of the mass of each tissue, and the hours of day/night period. As such, intracellular fluxes are in the units of mmol/g tissue/h, and boundary and inter-compartment fluxes are in the units of mmol/g leaf/h.

$$S_{C4\,leaf} = \begin{bmatrix}
S_{MD} & 0 & 0 & 0 & E_{MD} & 0 & 0 & 0 & \omega_{MD}^{-1} & 0 & 0 & 0 & \omega_{MD}^{-1} & 0 & 0 & 0 \\
0 & S_{MN} & 0 & 0 & 0 & E_{MN} & 0 & 0 & 0 & 0 & \omega_{MN}^{-1} & 0 & 0 & \omega_{MN}^{-1} & 0 & 0 \\
0 & 0 & S_{BD} & 0 & 0 & 0 & E_{BD} & 0 & 0 & \omega_{BD}^{-1} & 0 & 0 & 0 & 0 & \omega_{BD}^{-1} & 0 \\
0 & 0 & 0 & S_{BD} & 0 & 0 & 0 & E_{BN} & 0 & 0 & 0 & \omega_{BN}^{-1} & 0 & 0 & 0 & \omega_{BN}^{-1} \\
0 & 0 & 0 & 0 & 0 & 0 & 0 & 0 & CP & CP & 0 & 0 & 0 & 0 & 0 & 0 \\
0 & 0 & 0 & 0 & 0 & 0 & 0 & 0 & 0 & 0 & CP & CP & 0 & 0 & 0 & 0 \\
0 & 0 & 0 & 0 & 0 & 0 & 0 & 0 & 0 & 0 & 0 & 0 & SP & SP & 0 & 0 \\
0 & 0 & 0 & 0 & 0 & 0 & 0 & 0 & 0 & 0 & 0 & 0 & 0 & 0 & SP & SP
\end{bmatrix} \quad (1)$$

$$E_{\text{spatialtemporal}} = \omega_{spatialtemporal}^{-1} \cdot E \quad (2)$$

The area and volume ratios of M and B varies depending on the type of C_4 grass [34]. Here, we have assumed a 3:1 ratio of M:B to make an approximation for sugarcane leaves. The diurnal cycle was represented as 12 h day and 12 h night. Note that compartment weightings can alter input-output fluxes through the biomass drains.

The flux solution space of the C_4 leaf model was explored by flux balance analysis (FBA) [35] (Eq. (3)) (Fig. 2B). Briefly, linear programming was used to calculate flux distributions v based on flux boundary constraints v_{lb} and v_{ub}, and an objective function f . The

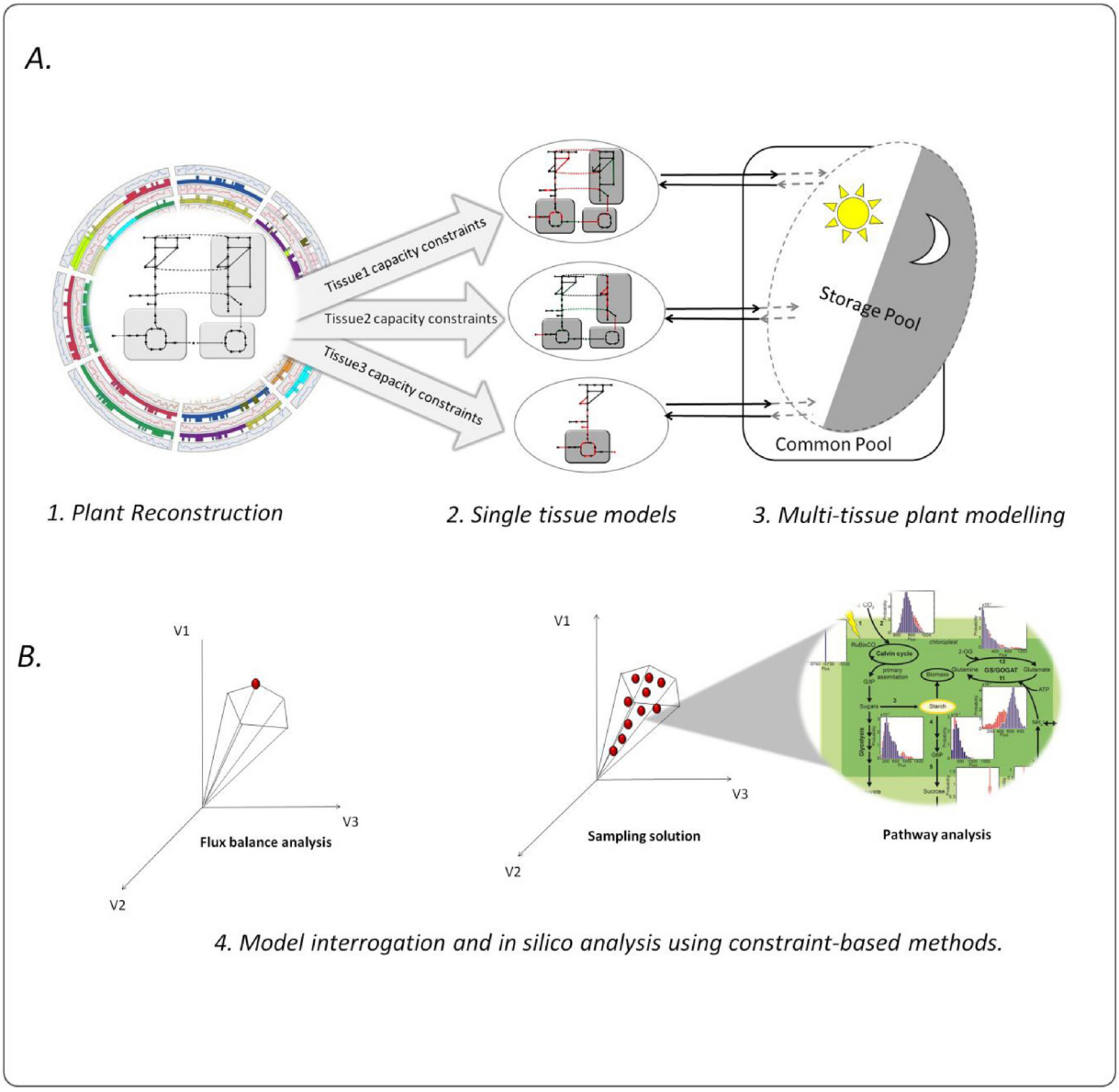

Fig. 2. Use of reconstruction, multi-tissue modelling (Multi-GEM) and constraint-based methods to interrogate plant metabolism. (A) From genome-scale reconstruction to multi-tissue modelling implementation. Step 1: Reconstruction is built based on plant genome annotation and plant biochemistry. The reconstruction network represents the metabolic capabilities of all the tissues. Step 2: The plant reconstruction is constrained and the network is reduced to represent tissue-specific metabolic capabilities. Step 3: tissues are connected by introducing a common pool, which represents the metabolites exchanged between the tissues. Temporal storage is introduced as a storage pool to model multi-tissue metabolism over the diurnal period. (B) Model interrogation. Step 4: multiple constraint-based methods are used for overall pathway analysis and to guide targets for metabolic engineering.

boundary and objective values can be controlled by users in the "model specification" spreadsheet (see Supplementary File S5, MultiGEM package).

$$\begin{aligned} &\min f.v \\ &S_{C4leaf}.\ v = 0 \\ &v_{lb} \le v \le v_{ub} \end{aligned} \tag{3}$$

Hypothesis testing consisted of a sequence of FBAs, with results from one FBA fed into the next FBA as constraints. The objective and boundary values were thus progressively modified to create the metabolic scenario required to address the hypothesis in question. For example, to find the maximum PHB production when photon uptake is increased by 5%, the minimum photon uptake required for wild-type growth is calculated first, and then the maximum PHB production is calculated after setting the photon uptake boundary value to 105% of the wild-type value. Hypothesis testing was conducted programmatically in MATLAB. The same can be accomplished using MultiGEM, although the procedure is cumbersome because MultiGEM creates a single instance of constraints and objective at a time.

The main objective function used in C_4 leaf FBA is "minimum photon uptake". For a photosynthetic system the logical optimality criterion is to maximise photon efficiency during growth [17,26,27,36]. For our purpose, this objective was applied mainly to establish a reference case. For fixed amounts of PHB and biomass, the optimisation with utilise the network such that total photon uptake is the least. We maintained this throughout our analyses to establish comparable scenarios.

Upon duplicating AraGEM in four spatio-temporal compartments, flux constraints were applied to differentiate them. To refine carbon assimilation pathways (Fig. 1), RuBisCO in M, and PEPC and CO_2 uptake in B were inactivated. Additionally, we eliminated starch storage

to B, direct conversion of pyruvate to oxaloacetate, free inter-conversion between NADH and NADPH, and photon uptake during night. Both linear and cyclic photosystems for M and B are assumed to be active. We lacked precise data to partition their contributions to ATP and NADPH generation, as their activities alter depending on condition and demand [37]. Optimisation was used to determine the most efficient configuration.

The specific constraints and objectives for each metabolic scenario are described together with the results. In general, we (i) quantified the metabolic cost of producing PHB at yields ranging from 1 to 10% g/g DW leaf, (ii) tested various metabolic penalties on PHB production (*e.g.*, photon assimilation deficiency, restricted plasmodesmata exchange metabolites and reduced carbon reserves) [9,12], and (iii) identified the preferred compartment to synthesise PHB.

2.4. Flux coupling and pathway analysis

Uniform random sampling of the flux solution space has been increasingly used for studying the correlation structure of metabolic networks [38–40], and the consequences of metabolic defects on the overall state of the network (*e.g.*, enzymopathies, inhibitors, *etc.*) [41,42]. Importantly, this technique enables identification of non-trivial couplings between reactions in different spatiotemporal compartments, enabling the appraisal of higher-order interactions [39].

In this work, the Artificially Centered Hit- and-Run (ACHR) algorithm [43] implemented in the ll-ACHRB package [39] was employed. This sampling algorithm is a robust uniform sampler that generates uniform random flux samples from metabolic models without the presence of active infeasible loops. These loops constitute thermodynamically infeasible cycles that carry flux without the energy expenditure, thereby contradicting the second law of thermodynamics [44]. Due to the complexity and relatively high number of potentially active infeasible loops in the C_4 leaf model (54), ll-ACHRB struggled to generate 'loopless' flux samples, and thus, we opted to disable the infeasible loop removal option. Despite this inconvenience, it is worth noting that, even without removing the infeasible loops, uniform sampling provides valuable insights into the emergent properties of plant metabolic networks (refer to Ref. [21]). Prior to sampling, all blocked reactions were removed from the model. These reactions represent reactions that can never carry a nonzero flux under the studied metabolic scenarios, and as such, they would never appear active in any metabolic pathway. Once the model was pre-processed, the sampling algorithm was executed and $5{\cdot}10^5$ flux samples were generated. In order to reduce serial autocorrelation, flux samples were taken every 200 steps (thinning) and the initial 10% of the sampling run was discarded as burn-in. Finally, the pairwise Pearson correlation coefficient (ρ) was calculated using this sample to determine the coupling degree between reactions.

A sparse representation of the null space of the stoichiometric matrix (S_{C4leaf}) yields a biologically meaningful and modular representation of the cell's metabolism consistent with biomolecular interactions [45]. Motivated by these capabilities, we constructed a sparse representation of the null space of the stoichiometric matrix (here denoted N_{C4leaf}) to reveal relevant pathways involved in PHB production and their interactions with the rest of plant metabolism. Notably, this representation is generated purely based on stoichiometry and directionalities, not on specific flux values, and as such, enables appraisal of emergent structural relationships within metabolism. To calculate N_{C4leaf}, we adapted an efficient algorithm for constructing a sparse representation of the minimal set of infeasible cycles in a metabolic model, Fast-SNP [44] – achieved by sparsifying the stoichiometric matrix of the internal reactions – to the generation of a sparse basis of the full solution space. Importantly, once N_{C4leaf} has been generated, one can describe any flux solution v^* as a linear combination (not necessarily positive) of the generating flux vectors or pathways $n_{C4leaf,i}$ contained in N_{C4leaf}. The weighting factor α_i by which $n_{C4leaf,i}$ contributes to a particular solution v^* is denoted the activity or "loading" of that particular pathway in v^* [45]. The higher the absolute value of α_i in v^*, the higher the activity of the corresponding pathway described by $n_{C4leaf,i}$. Following well-known results for orthogonal projections, the pathway activities were computed using,

$$\alpha = (N_{C4leaf}^T \cdot N_{C4leaf})^{-1} \cdot N_{C4leaf}^T \cdot v^*$$

2.5. Computational implementation

AraGEM was used as the base metabolic plant reconstruction for the implementation of the multi-tissue model [27]. The AraGEM reconstruction is not tissue specific and is organelle-compartmentalised to represent plant primary metabolism. Its network topology contains KEGG reaction identities that are homologue-mapped to Arabidopsis, sugarcane, maize, and switchgrass genes (Supplementary File S1) for comparative analysis. FBA and coupling calculations were performed using Gurobi Optimizer 5.6 (Gurobi Optimization, Inc.) within the MATLAB 2017a environment (The MathWorks, Natick, MA). MATLAB scripts, along with instructions of how to use the scripts, are provided in Supplementary File (MultiGEM package).

3. Results and discussion

3.1. Energy cost of PHB production differs slightly between organelles

Although successfully targeted in multiple organelles, the highest PHB levels (> 2% DW) in sugarcane and switchgrass have only been achieved in chloroplast-targeted lines [5,7]. Sugarcane leaves of peroxisome-targeted lines accumulated up to 1.6% PHB dry weight [15], whereas only trace amounts of PHB were detected in cytosol-targeted lines. In mitochondria-targeted lines, no PHB was detected [7]. Despite several efforts, there is still no obvious explanation as to why PHB was preferentially produced in chloroplasts, and not in other organelles like the mitochondria.

Qualitatively, the C_4 leaf model has provided an explanation. The default acetoacetyl-CoA reductase cofactor is NADPH, and experimental studies to date have only considered the overexpression of the NADPH isoenzyme [7]. As the linear photosystem can supply NADPH freely, optimisation results suggested that NADPH is best produced in B chloroplasts, and to transport NAPDH elsewhere will cost additional photons. AraGEM, without modification, could not produce NADPH in the mitochondria and peroxisome. Also, cytoplasmic NADPH is mainly produced by the oxidative pentose phosphate pathway, but in reality this pathway may be tightly coupled to ribose phosphate production for nucleotides. These connectivity and capacity limitations may explain why PHB production in the chloroplast is favoured over other organelles. To fix these limitations hypothetically in order to test all organelles, we manually added hypothetical NADH-dependent acetoacetyl-CoA reductase to the mitochondria and peroxisome.

The photon cost of PHB biosynthesis was different between organelles in the four spatiotemporal compartments: mitochondria ≪ plastid ≪ cytoplasm ≪ peroxisome in increasing order (Fig. 3A). Interestingly, producing PHB in mitochondria using NADH cost less photons than in chloroplast using NADPH. Because the TCA cycle must produce 2-oxoglutarate for biomass, the NADH generated by malate dehydrogenase, pyruvate dehydrogenase, and isocitrate dehydrogenase can supplement PHB production. This is potentially an attractive and viable strategy to redirect PHB production to the mitochondria, as this has been accomplished in yeast [46].

The increase in photon cost to produce PHB in less efficient organelles was significant in terms of PHB yield. Producing PHB at 3% DW in the best (mitochondrial, B, day) and the worst (peroxisome, B, night) compartments cost 1.63 and 2.57 mmol photon/g leaf/day, respectively. This is a 58% increase, suggesting that the compartment/

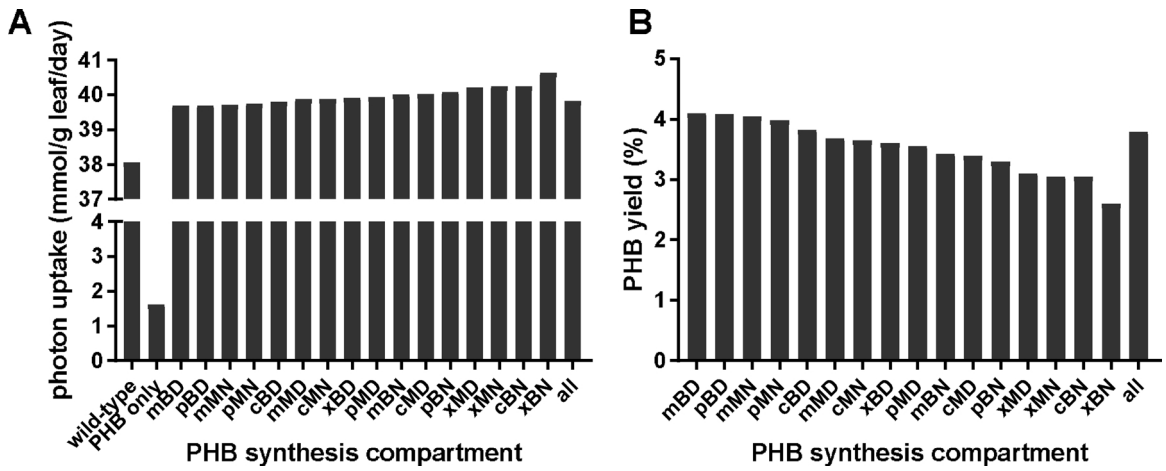

Fig. 3. Maximum production of PHB in 16 different spatiotemporal-organelle compartments. (A) Comparing photon uptake of PHB production to biomass in the different compartments (B) The maximum yields of PHB if starch and sucrose reserves were to be converted to PHB in the different compartments (tissue-organelle). m: mitochondria; p: plastid; c: cytosol; x: peroxisome; B: bundle sheath; M: mesophyll; D: day; N: night; all: all four spatiotemporal compartments in any organelle.

organelle of choice could potentially affect PHB yield. Flux simulations were accomplished by successively constraining the 16 PHB producing compartments to zero and finding the next best compartment to produce PHB.

The energetic burden of PHB production, however, was marginal relative to biosynthesis. Producing PHB at 3% DW (or 0.033 mmol PHB/g leaf/day) increased photon uptake by 4% to 7% depending on the compartments (relative to the photon demand of wild-type calculated at a growth rate of 0.11 day^{-1}). In fact, PHB production did not invoke any new reaction pathway beyond what is required for biosynthesis, apart from the five compartment-specific PHB pathway reactions (see Supplementary File S2). An exception is peroxisomal PHB production, which required 40 new reactions, but this was due to the use of fatty acid (C16) beta-oxidation to supply acetyl-CoA (and NADH) to the peroxisome.

Surprisingly, flux simulation revealed that M was the preferred tissue for PHB production during night (Fig. 3A). Photon cost to produce PHB during the day is additive, where biomass and PHB synthesis together are equal to the sum of the parts, *i.e.*, (X + Y) = X + Y. During the night, however, redox coupling gave some photon savings, *i.e.*, (X + Y) ≪ X + Y. PHB synthesis by itself cost 1.86 and 1.63 mmol photon/g leaf/day in mitochondria-M-night and mitochondria-B-day, respectively, but together with biomass the additional photon consumptions are 1.65 and 1.63 mmol photon/g leaf/day. PHB synthesis in M at night thus gave a photon saving of 0.21 mmol photon/g leaf/day. This is because M is more reliant on the TCA cycle to produce ATP for growth compared to B, which has first access to starch storage and hence preferentially utilises glycolysis.

As in many other fermentative systems, fine balancing of biosynthesis precursors, redox, and ATP is crucial. CO_2 is the only product during night metabolism, and the opportunity to produce PHB as a more reduced by-product means less carbon is lost by decarboxylation of acetyl-CoA *via* the TCA cycle. Biomass generation draws more oxidised precursors than PHB, thus PHB production provided additional means to counterbalance redox (as a sink). Night M relies on a full TCA cycle and respiration to produce ATP, but can now increase ATP generation by glycolysis, and concomitantly reduce succinate dehydrogenase (Complex II) activity (by half relative to wild-type). Interesting, in night B, the TCA cycle is not used directly to make ATP, indicated by an inactive succinate dehydrogenase. ATP is a by-product of converting pyruvate to 2-oxoglutarate for biosynthesis; glycolysis supplies the bulk of the ATP. During the day, the supply of redox and ATP is uncoupled by the cyclic and non-cyclic photophosphorylation pathways, hence the additive photon cost.

At PHB yield of 3% DW, flux simulations did not show a substantial energetic advantage when PHB is produced in B over M. Nonetheless, our results explained how certain organelles were preferred. Ultimately, however, these results did not explain why actual yields are persistently low. To address this, we next performed sensitivity analyses of PHB yields based on plausible physiological constraints and metabolic penalties inferred from experimental observations.

3.2. PHB yields limited by starch and sucrose reserves

Experimental studies of high PHB producer lines in both sugarcane and switchgrass showed depletion of carbon reserves in the form of starch and sucrose (Table 1) [6,10]. The amount of sucrose available for export from leaves (source) depends on several parameters: photosynthetic activity (carbon fixation), the portion consumed by starch synthesis and by triose phosphate export, and transient storage of sucrose in the vacuole [47,48]. Source-sink relationships are disrupted in engineered plant lines when one of these factors is altered [48]. A reduced carbon reserve over the diurnal cycle is likely to impact carbon available for storage, energy, and structure. As a consequence, plant growth deteriorates.

We questioned whether experimentally determined starch and sucrose reserves limited the maximum PHB yield. That is, PHB production can only access starch stored locally in the leaf, and not any alternative carbon sources that could be drawn from the stem. By stoichiometry, we calculated the maximum yield of PHB if all of these reserves were converted into PHB. First, we revised the starch and sucrose composition in the biomass equation of AraGEM to values measured for wild-type sugarcane (Table 1), and then calculated the minimum photon uptake without PHB production. Next, we calculated the maximum PHB production in each compartment with the minimum photon uptake and with starch and sucrose composition reduced to zero. Calculated PHB yields were between 3% and 4% (Fig. 3B), which is consistent with experimental measurements of 2–6% [5,6,10,11,16].

The consistency of predictions suggested that PHB production did not utilise carbon sources drawn from other plant tissues, making it plausible that PHB accumulation is limited by the availability of starch and sucrose reserves in leaf. These findings suggested that an increase in local carbon reserves is needed in order to sustain normal growth and to improve PHB yield. And perhaps, enhancing starch synthesis and storage in M may induce localised PHB production. In agreement with *in silico* analysis, it has been demonstrated in switchgrass that decreased C reserve content in high PHB producers [10] was alleviated by increasing carbon flow through photosynthesis [13].

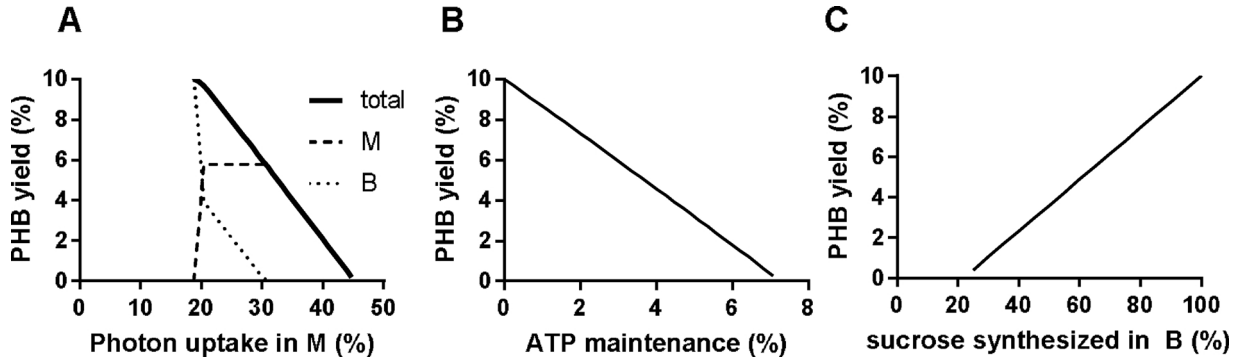

Fig. 4. Sensitivity analysis of PHB yield. The correlation of PHB yield with (A) photon uptake in M, (B) ATP maintenance, and (C) sucrose synthesis in B.

3.3. Potential metabolic penalties that reduce PHB yields

Increasing PHB yields from 1% to 10% showed that PHB production is coupled linearly to photoassimilation capacity. This is because photosynthesis must generate NADPH and ATP consumed by PHB synthesis (Supplementary File S2). If a "super producer" with 10% PHB yield is indeed possible, then what are the hidden metabolic penalties that could reduce yields to 3% as observed experimentally?

We explored (i) the partitioning of photosynthesis between B and M (as both are photosynthetic cells), (ii) ATP maintenance, and (iii) metabolites used in plasmodesmata exchange. These unknown parameters diminish PHB yields. While hard to quantify experimentally, their effects are readily simulated. Simulations were performed by fixing the allowable photon uptake to the 10% producer, and subsequently applying the relevant flux constraints in increasing magnitude until maximum PHB yield is reduced to zero.

3.3.1. M photosynthesis reduces overall PHB yield but diverts PHB production into M

Flux simulations showed that 81% of the photon uptake is by B, despite M possessing 70% of a leaf's photosynthetic area [34]. This phenotype is driven by the fact that both Calvin cycle and carbohydrate synthesis are most energetically efficient when co-localised, in B. Sensitivity analysis was performed by maximising PHB yield while reducing B photon uptake from 81% to the minimum value (Fig. 4A).

A slight diversion in photon uptake from B to M revealed two interesting features: PHB production was enabled in M, and M became the preferred synthesis compartment. The aforementioned redox coupling during night metabolism drives this feature. Previously, it was shown that photon consumption at 3% PHB yield was only marginally different between mitochondria-M-night and mitochondria-B-day (1.65 and 1.63 mmol photon/g leaf/day). Starch "fermentation" to PHB in the growing leaf milieu became more photon efficient at night when photon uptake was limiting in B. With decreasing photon uptake by B, carbon assimilation became an elaborate cycle between two leaf tissues, with B increasing glucose 6-phosphate synthesis from G3P and subsequent transport of sucrose into M, and with sucrose carbon returned as G3P to supply the Calvin cycle. This effectively shifted ATP-investment steps of glycolysis into M to absorb the increasing ATP production in M by the cyclic photosystem. However, the shunting of carbon substrates around costs energy, as reflected by the diminishing total PHB yield.

The PHB yield was eventually reduced to zero when M photon uptake was at 45% of total. If 70% is representative of physiological contribution of M, then the current simulations suggested that shifting ATP production from B into M can significantly penalise PHB production. However, the results also revealed that starch catabolism could be leveraged to enhance PHB production in mesophyll (*i.e.*, over-production of starch storage during the day).

3.3.2. ATP maintenance is a significant competitor for photons

Next, we evaluated the cost of ATP maintenance in magnitude equivalent to PHB yield (Fig. 4B). The fluxes of ATP hydrolysis reactions (R00086) in all four compartments were increased gradually to represent ATP maintenance, with the sum of hydrolysis fluxes expressed as a percentage of the total ATP produced in the leaf (Supplementary File S2, sim1 > scenarios 26–32). At 5.13%, ATP maintenance reduced PHB yield from 10% to 3%. This indicated that unaccounted maintenance demand is a potential competitor for ATP relative to PHB production. The greatest impact on carbon flow was incurred during night metabolism, with both tissues increasing oxidative respiration to counteract ATP maintenance. Interestingly, M increased TCA cycle activity, but B relied on glycolysis to generate NADH for ATP production. During the day, non-cyclic photophosphorylation was engaged instead because the cyclic photosystem is more efficient at producing ATP than the respiratory chain.

3.3.3. Sucrose as the preferred metabolite exchanged through plasmodesmata

Flux simulation consistently placed carbohydrate synthesis in B where the Calvin cycle is active. Interestingly, in the attempt to maximise photon efficiency, the linear photosystem (NADPH production) in B was engaged but not in M, with NAPDH shuttled from B to M *via* sucrose. As the majority of sucrose in *Zea mays* is synthesised in M [49], this raised the concern that PHB yield is affected by tissue localisation of sucrose synthesis. Here, we constrained the flux through sucrose synthesis reaction (R00806) from maximum value of the 10% PHB producer until PHB yield reached zero.

In wild-type (model based reference), all sucrose is synthesised in B, with the majority exported to M. In M, sucrose is catabolised to G3P and 2PG, which were transported back into B. Gradually decreasing sucrose synthesis in B to 25% reduced PHB yield to zero in a linear fashion (Fig. 4C). Interestingly, this reduction was not compensated by an increase in carbohydrate synthesis in M. Instead, G3P transport from B to M was increased, with 2PG recycled back into B, but ATP produced from glycolysis was reduced. Cyclic photophosphorylation in M was increased to make up for the shortfall of ATP, but this diverted photon away from B, thus reducing overall photoassimilation capacity and PHB yield.

Metabolites are exchanged through the plasmodesmata freely, driven by concentration gradients dictated by the activities of pathways in B and M. These metabolites have varying payloads in terms of carbon, ATP, and redox. Simulations suggested that M relied on glycolysis of sucrose to produce NADH and ATP, instead of the photosystem. Carbohydrate synthesis is preferred in B because the Calvin cycle bypasses the fructose-1,6-bisphosphatase reaction. While G3P can substitute sucrose, it is energetically less efficient because it does not take advantage of this ATP-conserving step available only in B.

Table 2
Main features of minimal PHB-producing pathways.

Pathway number (ID)[a]	Length	$Y_{PHB,hv}$	Starch reserve involved	v_{PHB} compartment	v_{PHB} period	Organelles involved in pathway[b]		
						c	m	p
597 (5)	106	0.020	NO	B, m	D	x	x	x
611 (16)	97	0.019	NO	B, p	D	x	x	x
602 (9)	120	0.018	NO	B, c	D	x	x	x
320 (2)	170	0.016	NO	B, x	D	x	x	x
612 (17)	198	0.018	YES	B, p	N	x	x	x
600 (7)	234	0.013	YES	B, m	N	x	x	x
546 (3)	288	0.012	YES	B, x	N	x	x	x
595 (4)	206	0.006	YES	B, c	N	x	x	x
601 (8)	227	0.007	YES	B, m	N	x	x	x
605 (11)	171	0.017	NO	M, x	D	x	x	x
610 (15)	101	0.017	NO	M, p	D	x	x	x
603 (10)	98	0.015	NO	M, m	D	x	x	x
613 (18)	112	0.009	NO	M, c	D	x	x	x
606 (12)	269	0.018	YES	M, x	N	x	x	x
615 (19)	212	0.018	YES	M, c	N	x	x	x
598 (6)	299	0.014	YES	M, x	N	x	x	x
169 (1)	176	0.013	YES	M, p	N	x	x	x
609 (14)	149	0.012	YES	M, m	N	x	x	x

[a] The number in parenthesis denotes the corresponding ID of the pathway shown in Supplementary File S4.
[b] This column indicates the presence of reactions from different compartments in the analysed pathway (m: mitochondria, p: plastid; c: cytoplasm; x: peroxisome). An 'x' indicates the involvement of the corresponding organelle in the pathway.

3.4. Topological and sampling analysis supports dependency of PHB production on photoassimilation

To better understand the consequences of PHB production in bioenergy grasses, topological and sampling analyses were employed to reveal structural and coupling relationships between metabolic pathways and reactions across different tissues over the diurnal cycle. As a case study, we modelled the metabolism of a 3% leaf DW PHB producer. Sampling was performed assuming: (i) a nearly optimal photon usage (1% flexibility was allowed with respect to the minimal photoassimilation), and (ii) a fixed biomass growth equal to the wild-type value [11]. Also, an additional PHB drain reaction was included in the model that concentrates all the PHB produced in the different spatiotemporal compartments. The flux through this reaction was fixed so that a 3% PHB DW yield in leaf was reached. In this way, the model was allowed to freely choose between the different cell types, organelles, and periods, to reach the biomass and PHB production levels under the (near) optimal photoassimilation constraint.

3.4.1. Core pathways supporting PHB production

The full space of the C_4 model can be decomposed into 638 minimal linearly-independent pathways. Of these pathways, 19 represent the pathways of PHB production in different tissues-diurnal compartments (MD, MN, BD, and BN), and involve reactions from all organelles (c,m,p,x) (Table 2 and Supplementary File S3). In total they spanned ~15% of the reactions (1001) in the C_4 model. The relatively long pathways suggested that PHB production is dependent on numerous central metabolic processes, with 52 reactions common to all PHB-producing pathways. These reactions encompass various metabolic processes such as metabolite transport/translocation, sugar metabolism (glycolysis and gluconeogenesis), carbon fixation, and photoassimilation (Supplementary File S3 Table S1). As expected, all PHB-producing pathways were coupled to the photoassimilation reaction in either tissue (M,B) and period (D,N) (Supplementary File S4). PHB production was thus highly coupled to the leaf's photoassimilation capacity as previously determined through optimisation, and confirmed experimentally [13]. Twelve out of the 19 PHB pathways utilised starch production because these pathways are linked to PHB production at night (Table 2). The observed coupling to beta-oxidation is due to a lack of direct transport of cytosolic acetyl-CoA into the peroxisome.

3.4.2. Uniform sampling revealed the extent of PHB production preference in different spatiotemporal compartments and relevant coupling relationships

In order to gain a deeper insight into the consequences of PHB production in the metabolism of C_4 plants across the diurnal cycle, uniform random samples were generated to explore the flux coupling structure between reactions in each spatiotemporal compartment. The flux correlation structure showed strong coupling within each spatiotemporal compartment and weak coupling between reactions of different spatiotemporal compartments (Fig. 5A). In contrast to the flux correlation structure, the pathway activity correlation landscape showed greater interconnectivities and with pathways more tightly correlated (Fig. 5B).

Firstly, we analysed reactions strongly coupled ($|\rho| > 0.5$) to PHB production. Results indicated that PHB production did not belong to a single compartment or period, but was associated with very specific metabolic processes, mainly starch metabolism (C reserve) and PHB synthesis. In the latter case, two enzymatic reactions consistently display strong coupling with PHB production in every spatiotemporal compartment: acetoacetyl-CoA reductase, and 3-ketoacyl-CoA thiolase (both from $|\rho| = 0.57$ up to $|\rho| = 0.71$, Supplementary File S3 Tables S2–S5). These enzymatic steps represent the commitment steps to PHB production. 3-Ketoacyl-CoA thiolase has been demonstrated to be the rate-limiting step of PHB production given its relatively high thermodynamic cost ($\Delta G^0_r = 7$ kcal/mol), which can be overcome by replacing it with the more thermodynamically favoured acetoacetyl-CoA synthase ($\Delta G^0_r = -0.9$ kcal/mol) [50]. Interestingly, depending on when and where PHB is produced (bundle sheath or mesophyll and day or night period), the 3-ketoacyl-CoA thiolase often should be downregulated in another cell type and/or period to improve PHB production, supporting the idea that PHB is more efficiently produced in a single spatiotemporal compartment. Analysis of the flux probability distributions confirmed this claim, supporting PHB production in bundle sheath during day over the mesophyll during night (p-value $\ll 10^{-32}$ Wilcoxon rank sum test, Fig. 6A), and also highlighted a statistically significant difference in PHB production between the tissues and periods (p-value $\ll 10^{-32}$, ANOVA test).

Finally, analysis of the activity profile of the PHB-producing pathways showed a clear preference for the highest PHB-yield production pathway (Pathway ID 597, Fig. 6B). Interestingly, this highly active pathway displayed the exact opposite activity profile compared to the

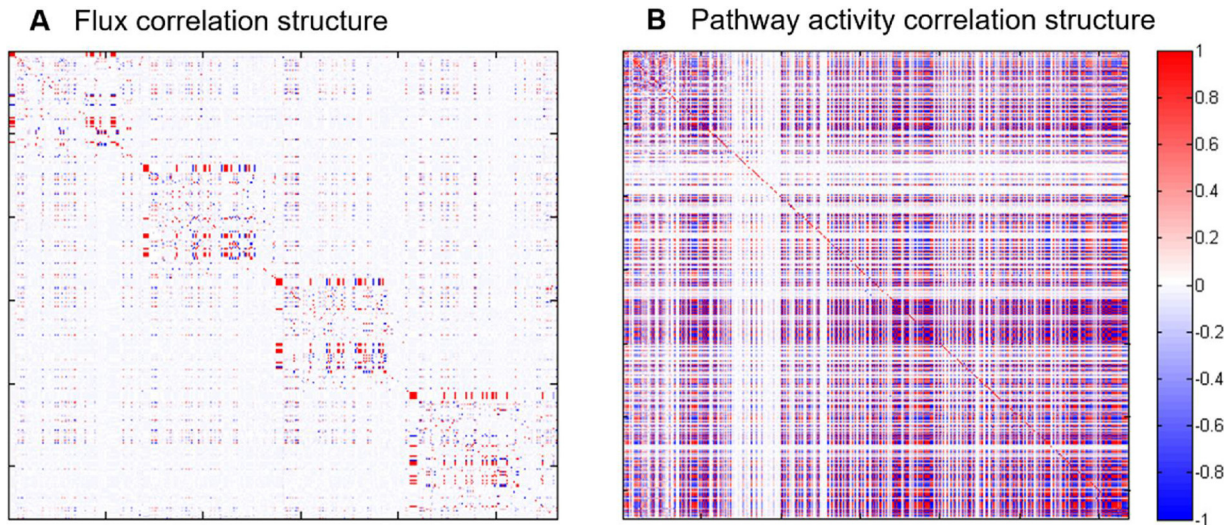

Fig. 5. Flux and pathway activity correlation structures. These heatmaps describe the Pearsons' correlation coefficients between all the reactions (A) and pathways (B) present in the C_4 leaf model estimated using flux random sampling. While model reactions display a stronger coupling within each spatiotemporal compartment as shown by the diagonal pattern, the pathway activity correlation structure exhibits a far more inter-connected pattern, highlighting the inter-dependence between organelles, tissues and time periods, in a PHB-producing plant line.

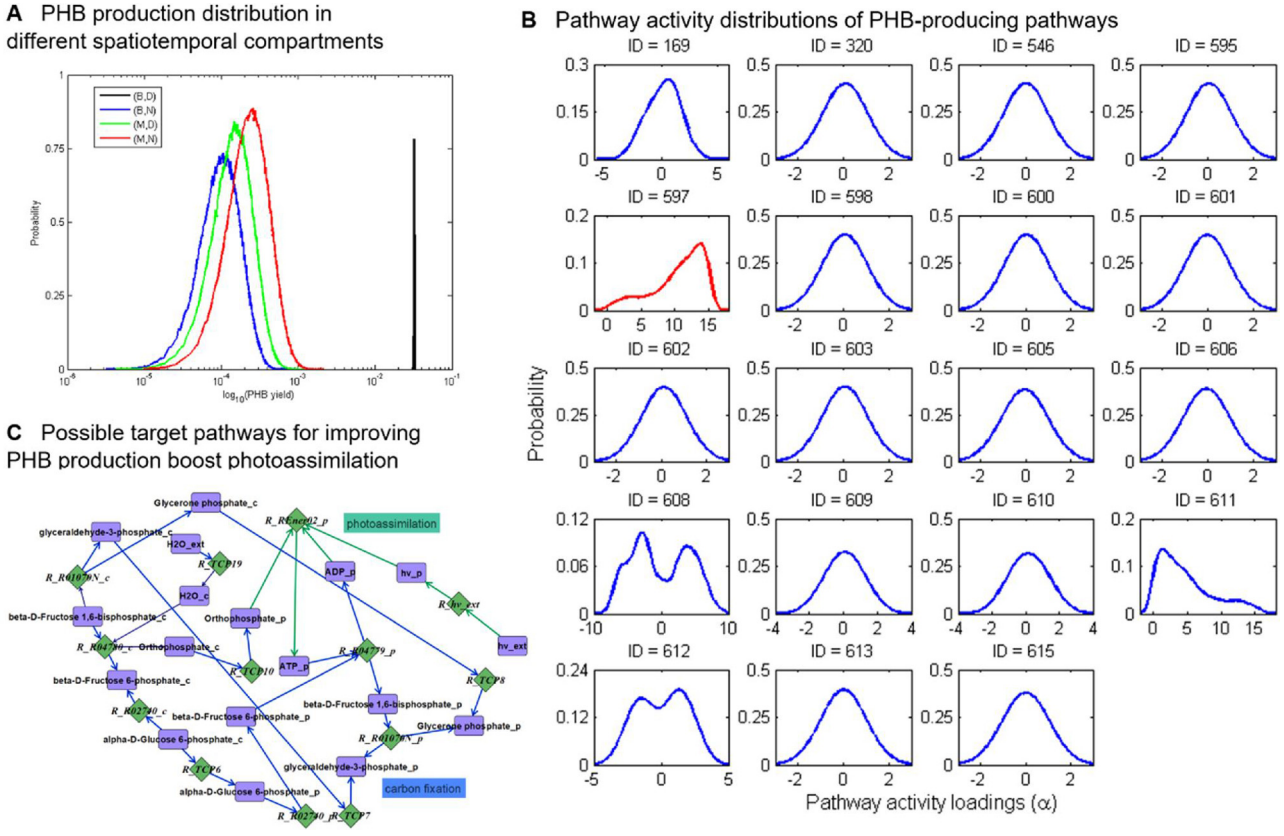

Fig. 6. Random sampling reveals preferred spatiotemporal compartments for high PHB production in a PHB-producing cell line. (A) Flux probability distributions of PHB-producing reactions in different spatiotemporal compartments. Production in bundle sheath during the day (B,D) is the preferred spatiotemporal compartment as shown by its higher flux. (B) Pathway loadings of the different PHB-producing pathways. Shown in red, the pathway with the highest activity or loading in the high PHB production phenotype. (C) High-activity pathway for high PHB production. Analysis of this pathway reveals metabolic targets for improving PHB accumulation. Targets related to an increased photoassimilation and carbon fixation are highlighted as convenient targets. (For interpretation of the references to colour in this figure legend, the reader is referred to the web version of this article.)

second highest PHB-producing pathway (Pathway ID 611, Fig. 6B). Coupling analysis between these pathways revealed that the latter compete for PHB production in bundle sheath during day period ($\rho = -0.99$, Supplementary File S2 Table S6). Ignoring this coupling, the top six pathways with the highest coupling to the two PHB-producing pathways with the highest yield not only were identical, but even shared the same ranking (Supplementary File S2 Table S6). These pathways were related to proton recycling (1), carbon fixation and

photoassimilation (2), nucleotide recycling (3), amino sugars regeneration (4) and amino acids metabolism (5). Among these, we disregarded four thermodynamically infeasible pathways. The two pathways remaining were directly related to photon uptake and carbon fixation in bundle sheath during day, but contain possible futile cycles (Fig. 6C) (Supplementary File S2 Table S7). These two high-activity pathways reinforced the need for increased photoassimilation for higher PHB accumulation. More experimental investigations targeting carbon assimilation and photoassimilation pathways in new PHB producers are needed to validate these findings.

4. Conclusion

The combined use of reconstruction, modelling, and *in silico* pathway analysis illustrates the potential of using genome-scale models to explore carbon partitioning and metabolic engineering problems. The framework made it possible to evaluate the impact of metabolic constraints on resource allocation in mesophyll and bundle sheath cell during the day (synthesis) and night (respiration) when a novel carbon sink is added in C_4 leaves. Overall, flux simulations and pathway analyses showed that up-regulation of photoassimilation is required to restore carbon reserves and to improve PHB production. This is because PHB is a direct competitor of leaf biomass for carbon, redox, and ATP. Sampling analysis revealed patterns of reactions and pathways that were correlated with the PHB extra sink. The method enabled us to create a 'pathway library' which reveals enzymatic reactions that are strongly correlated to the desirable phenotype, *i.e.*, high PHB production. These results show the potential of using metabolic reconstruction, multi-tissue modelling and sampling to improve the understanding of the potential metabolic limitations and penalties that impinge on PHB production, and to generate a shortlist of pathways that should be targeted to improve PHB yield. Finally, MultiGEM provides a convenient framework to explore C_4 leaf metabolism.

Acknowledgments

We thank Yield 10 Bioscience, Inc. and Metabolix, Inc. for the support received to develop this work.

Appendix A. Supplementary data

Supplementary data associated with this article can be found, in the online version, at https://doi.org/10.1016/j.plantsci.2018.03.027.

References

[1] R.A. Kennedy, W.M. Laetsch, Plant species intermediate for C3, C4 photosynthesis, Science 184 (4141) (1974) 1087–1089.
[2] P.D. Moore, C3,C4 – mechanisms, and cellular and environmental-regulation, of photosynthesis – Edwards, G, Walker, D, Nature 308 (5955) (1984) 124.
[3] M.D. Hatch, T. Kagawa, Photosynthetic activities of isolated bundle sheath-cells in relation to differing mechanisms of C4 pathway photosynthesis, Arch. Biochem. Biophys. 175 (1) (1976) 39–53.
[4] T. Jenkins, A. Bovi, R. Edwards, Plants: biofactories for a sustainable future? Philos. Trans. R. Soc. A 369 (1942) (2011) 1826–1839.
[5] M.N. Somleva, et al., Production of polyhydroxybutyrate in switchgrass, a value-added co-product in an important lignocellulosic biomass crop, Plant Biotechnol. J. 6 (7) (2008) 663–678.
[6] L.A. Petrasovits, et al., Enhanced polyhydroxybutyrate production in transgenic sugarcane, Plant Biotechnol. J. 10 (5) (2012) 569–578.
[7] L.A. Petrasovits, et al., Production of polyhydroxybutyrate in sugarcane, Plant Biotechnol. J. 5 (1) (2007) 162–172.
[8] X.F. Wang, et al., Production of polyhydroxybuyrate (PHB) from switchgrass pretreated with a radio frequency-assisted heating process, Biomass Bioenergy 94 (2016) 220–227.
[9] C.G. de Oliveira Dal'Molin, et al., Metabolic reconstruction of *Setaria italica*: a systems biology approach for integrating tissue-specific omics and pathway analysis of bioenergy grasses, Front. Plant Sci. 7 (2016) 1138.
[10] R.B. McQualter, et al., Systems biology and metabolic modelling unveils limitations to polyhydroxybutyrate accumulation in sugarcane leaves; lessons for C4 engineering, Plant Biotechnol. J. 14 (2) (2016) 567–580.
[11] R.B. McQualter, et al., Factors affecting polyhydroxybutyrate accumulation in mesophyll cells of sugarcane and switchgrass, BMC Biotechnol. 14 (2014) 83.
[12] R.B. McQualter, et al., The use of an acetoacetyl-CoA synthase in place of a beta-ketothiolase enhances poly-3-hydroxybutyrate production in sugarcane mesophyll cells, Plant Biotechnol. J. 13 (5) (2015) 700–707.
[13] M.N. Somleva, O.P. Peoples, K.D. Snell, PHA bioplastics, biochemicals, and energy from crops, Plant Biotechnol. J. 11 (2) (2013) 233–252.
[14] M. Nageswara-Rao, et al., Advances in biotechnology and genomics of switchgrass, Biotechnol. Biofuels (2013) 6.
[15] K. Tilbrook, et al., Peroxisomal polyhydroxyalkanoate biosynthesis is a promising strategy for bioplastic production in high biomass crops, Plant Biotechnol. J. 9 (9) (2011) 958–969.
[16] L.A. Petrasovits, et al., Chemical inhibition of acetyl coenzyme A carboxylase as a strategy to increase polyhydroxybutyrate yields in transgenic sugarcane, Plant Biotechnol. J. 11 (9) (2013) 1146–1151.
[17] C.G. de Oliveira Dal'Molin, L.K. Nielsen, Plant genome-scale metabolic reconstruction and modelling, Curr. Opin. Biotechnol. 24 (2) (2013) 271–277.
[18] S.Y. Lee, D. Mattanovich, A. Villaverde, Systems metabolic engineering, industrial biotechnology and microbial cell factories, Microb. Cell Fact. 11 (2012) 156.
[19] J.W. Lee, et al., Systems metabolic engineering of microorganisms for natural and non-natural chemicals, Nat. Chem. Biol. 8 (6) (2012) 536–546.
[20] Y.L. Wang, J.A. Eddy, N.D. Price, Reconstruction of genome-scale metabolic models for 126 human tissues using mCADRE, BMC Syst. Biol. (2012) 6.
[21] C.G. de Oliveira Dal'Molin, et al., A multi-tissue genome-scale metabolic modeling framework for the analysis of whole plant systems, Front. Plant Sci. 6 (2015) 4.
[22] R.T. Furbank, C.L.D. Jenkins, M.D. Hatch, The Co2 concentrating function of C4 photosynthesis, Curr. Res. Photosynth. 1–4 (1990) D541–D544 3812.
[23] F. Pfundel, B. Neubohn, Assessing photosystem I and II distribution in leaves from C-4 plants using confocal laser scanning microscopy, Plant Cell Environ. 22 (12) (1999) 1569–1577.
[24] S.R. Spilatro, J. Preiss, Regulation of starch synthesis in the bundle sheath and mesophyll of *Zea-mays*-L. – intercellular compartmentalization of enzymes of starch metabolism and the properties of the adpglucose pyrophosphorylases, Plant Physiol. 83 (3) (1987) 621–627.
[25] H. Poorter, M. Bergkotte, Chemical-composition of 24 wild-species differing in relative growth-rate, Plant Cell Environ. 15 (2) (1992) 221–229.
[26] C.G. de Oliveira Dal'Molin, et al., AraGEM, a genome-scale reconstruction of the primary metabolic network in Arabidopsis, Plant Physiol. 152 (2) (2010) 579–589.
[27] C.G. de Oliveira Dal'Molin, et al., C4GEM, a genome-scale metabolic model to study C4 plant metabolism, Plant Physiol. 154 (4) (2010) 1871–1885.
[28] T.C. Williams, et al., A genome-scale metabolic model accurately predicts fluxes in central carbon metabolism under stress conditions, Plant Physiol. 154 (1) (2010) 311–323.
[29] S. Mintz-Oron, et al., Reconstruction of *Arabidopsis* metabolic network models accounting for subcellular compartmentalization and tissue-specificity, Proc. Natl. Acad. Sci. U. S. A. 109 (1) (2012) 339–344.
[30] C.Y.M. Cheung, et al., A diel flux balance model captures interactions between light and dark metabolism during day-night cycles in C3 and crassulacean acid metabolism leaves, Plant Physiol. 165 (2) (2014) 917–929.
[31] M. Lakshmanan, et al., Unraveling the light-specific metabolic and regulatory signatures of rice through combined in silico modeling and multiomics analysis, Plant Physiol. 169 (4) (2015) 3002–3020.
[32] V. Baldazzi, et al., Towards multiscale plant models: integrating cellular networks, Trends Plant Sci. 17 (12) (2012) 728–736.
[33] C. Gomes de Oliveira Dal'Molin, L.K. Nielsen, Plant genome-scale reconstruction: from single cell to multi-tissue modelling and omics analyses, Curr. Opin. Biotechnol. 49 (2017) 42–48.
[34] P.W. Hattersley, Characterization of C-4 type leaf anatomy in grasses (Poaceae), mesophyll – bundle sheath area ratios, Ann. Bot. 53 (2) (1984) 163–179.
[35] J.D. Orth, I. Thiele, B.O. Palsson, What is flux balance analysis? Nat. Biotechnol. 28 (3) (2010) 245–248.
[36] C.G.O. de Oliveira Dal'molin, et al., Plant genome-scale modeling and implementation, Methods Mol. Biol. (Clifton, NJ) 1090 (2014) 317–332.
[37] G.N. Johnson, Physiology of PSI cyclic electron transport in higher plants, Biochim. Biophys. Acta Bioenergetics 1807 (3) (2011) 384–389.
[38] E. Almaas, et al., Global organization of metabolic fluxes in the bacterium *Escherichia coli*, Nature 427 (2004) 839–843.
[39] P.A. Saa, L.K. Nielsen, ll-ACHRB: a scalable algorithm for sampling the feasible solution space of metabolic networks, Bioinformatics 32 (15) (2016) 2330–2337.
[40] S. Bordel, R. Agren, J. Nielsen, Sampling the solution space in genome-scale metabolic networks reveals transcriptional regulation in key enzymes, PLoS Comput. Biol. 6 (7) (2010) e1000859.
[41] N.D. Price, J. Schellenberger, B.O. Palsson, Uniform sampling of steady-state flux spaces: means to design experiments and to interpret enzymopathies, Biophys. J. 87 (2004) 2172–2186.
[42] N.E. Lewis, et al., Large-scale in silico modeling of metabolic interactions between cell types in the human brain, Nat. Biotechnol. 28 (12) (2010) 1279–1291.
[43] D.E. Kaufman, R.L. Smith, Direction choice for accelerated convergence in hit-and-run sampling, Oper. Res. 46 (1) (1998) 84–95.
[44] P.A. Saa, L.K. Nielsen, Fast-SNP: a fast matrix pre-processing algorithm for efficient loopless flux optimization of metabolic models, Bioinformatics 32 (24) (2016) 3807–3814.
[45] A. Bordbar, et al., Minimal metabolic pathway structure is consistent with associated biomolecular interactions, Mol. Syst. Biol. 10 (2014) 737.
[46] A.M. de las Heras, et al., Anaerobic poly-3-D-hydroxybutyrate production from xylose in recombinant Saccharomyces cerevisiae using a NADH-dependent

acetoacetyl-CoA reductase, Microb. Cell Fact. (2016) 15.
[47] D.M. Braun, T.L. Slewinski, Genetic control of carbon partitioning in grasses: roles of sucrose transporters and tie-dyed loci in phloem loading, Plant Physiol. 149 (1) (2009) 71–81.
[48] R. Lemoine, et al., Source-to-sink transport of sugar and regulation by environmental factors, Front. Plant Sci. 4 (2013) 272.
[49] J.E. Lunn, R.T. Furbank, Localisation of sucrose-phosphate synthase and starch in leaves of C-4 plants, Planta 202 (1) (1997) 106–111.
[50] R.B. McQualter, et al., The use of an acetoacetyl-CoA synthase in place of a beta-ketothiolase enhances poly-3-hydroxybutyrate production in sugarcane mesophyll cells, Plant Biotechnol. J. 13 (5) (2015) 700–707.